CHALMERS

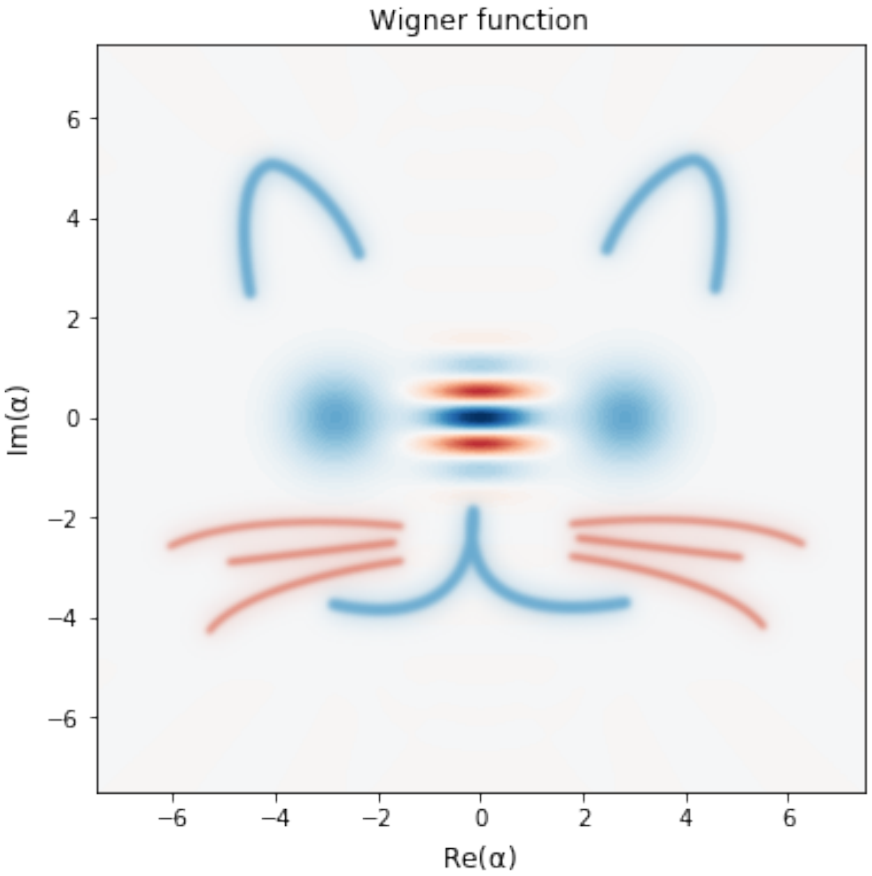

Cat State Preparation By Quantum Optimal Control with Krotov's Method

How to prepare your cat

Master's thesis in Quantum Computing

JOHAN WINTHER

Department of Microtechnology and Nanoscience
CHALMERS UNIVERSITY OF TECHNOLOGY
Göteborg, Sweden 2019

MASTER'S THESIS IN QUANTUM COMPUTING

Cat State Preparation By Quantum Optimal Control with Krotov's Method

How to prepare your cat

JOHAN WINTHER

Department of Microtechnology and Nanoscience
Division of Applied Quantum Mechanics
CHALMERS UNIVERSITY OF TECHNOLOGY

Göteborg, Sweden 2019

Cat State Preparation By Quantum Optimal Control with Krotov's Method
How to prepare your cat
JOHAN WINTHER

Master's thesis 2019:XX
ISSN 1652-8557
Department of Microtechnology and Nanoscience
Division of Applied Quantum Mechanics
Chalmers University of Technology
SE-412 96 Göteborg
Sweden
Telephone: +46 (0)31-772 1000

Cover:
Some explanation

Chalmers Reproservice
Göteborg, Sweden 2019

Cat State Preparation By Quantum Optimal Control with Krotov's Method
How to prepare your cat

JOHAN WINTHER
Department of Microtechnology and Nanoscience
Division of Applied Quantum Mechanics
Chalmers University of Technology

Abstract

Quantum computing has gained a lot of interest in recent years and commercial products are just now entering the market. However one of the main challenges in realising a quantum computer is noise and one key technology to remedy this is quantum error correction (QEC). One way of performing QEC is to store the quantum information of a qubit, while it's idle, as special basis states in a resonator. To do this one needs to apply encoding and decoding pulses to the coupled qubit-resonator system to do a state transfer. These pulses are hard or perhaps impossible to solve for analytically, which means they need to be numerically obtained by simulation.

This thesis studies the prospects of using Krotov's method (gradient ascent) to numerically optimize encoding pulses for state transfer. The Python package Krotov, a package for quantum optimal control using Krotov's method, is used to perform state transfers $|0\rangle$ to $|1\rangle$ and $|0\rangle$ to $|2\rangle$ of an anharmonic resonator. It is shown that, assuming a maximum drive amplitude and no dissipation, the method can realise a $|0\rangle$ to $|1\rangle$ transfer with fidelity $F > 0.99999$ with a total pulse length of only 10.75 ns. For the $|0\rangle$ to $|2\rangle$ transfer a total pulse length of 30 ns is needed to reach the same fidelity. Thus it is concluded that state transfers using Krotov for non-coupled systems is viable.

However for coupled systems there is great difficulty in using Krotov, as the package assumes a time-independent control Hamiltonian. A potential workaround for this problem is also presented.

Keywords: quantum computing, quantum optimal control, cat state, cat code

Sammanfattning

Preface

Acknowledgements

I would like to thank

Nomenclature

Lorem ipsum dolor sit amet, consectetuer adipiscing elit. Ut purus elit, vestibulum ut, placerat ac, adipiscing vitae, felis. Curabitur dictum gravida mauris. Nam arcu libero, nonummy eget, consectetuer id, vulputate a, magna. Donec vehicula augue eu neque. Pellentesque habitant morbi tristique senectus et netus et malesuada fames ac turpis egestas. Mauris ut leo. Cras viverra metus rhoncus sem. Nulla et lectus vestibulum urna fringilla ultrices. Phasellus eu tellus sit amet tortor gravida placerat. Integer sapien est, iaculis in, pretium quis, viverra ac, nunc. Praesent eget sem vel leo ultrices bibendum. Aenean faucibus. Morbi dolor nulla, malesuada eu, pulvinar at, mollis ac, nulla. Curabitur auctor semper nulla. Donec varius orci eget risus. Duis nibh mi, congue eu, accumsan eleifend, sagittis quis, diam. Duis eget orci sit amet orci dignissim rutrum.

Nam dui ligula, fringilla a, euismod sodales, sollicitudin vel, wisi. Morbi auctor lorem non justo. Nam lacus libero, pretium at, lobortis vitae, ultricies et, tellus. Donec aliquet, tortor sed accumsan bibendum, erat ligula aliquet magna, vitae ornare odio metus a mi. Morbi ac orci et nisl hendrerit mollis. Suspendisse ut massa. Cras nec ante. Pellentesque a nulla. Cum sociis natoque penatibus et magnis dis parturient montes, nascetur ridiculus mus. Aliquam tincidunt urna. Nulla ullamcorper vestibulum turpis. Pellentesque cursus luctus mauris.

Nulla malesuada porttitor diam. Donec felis erat, congue non, volutpat at, tincidunt tristique, libero. Vivamus viverra fermentum felis. Donec nonummy pellentesque ante. Phasellus adipiscing semper elit. Proin fermentum massa ac quam. Sed diam turpis, molestie vitae, placerat a, molestie nec, leo. Maecenas lacinia. Nam ipsum ligula, eleifend at, accumsan nec, suscipit a, ipsum. Morbi blandit ligula feugiat magna. Nunc eleifend consequat lorem. Sed lacinia nulla vitae enim. Pellentesque tincidunt purus vel magna. Integer non enim. Praesent euismod nunc eu purus. Donec bibendum quam in tellus. Nullam cursus pulvinar lectus. Donec et mi. Nam vulputate metus eu enim. Vestibulum pellentesque felis eu massa.

Contents

1 Introduction

Quantum computing is starting to appear in commercial products [1], however, despite a lot of progress [2], there are still a lot of challenges to be solved before large scale quantum computers become commonplace. Unlike classical computers, where the transistors' on and off state is dictated by the stream of many electrons, quantum computers rely on single or very few number of particles which make the quantum states very delicate [3].

One of the key technologies to keep these states in quantum computing is quantum error correction (QEC) [3], which is a way to retain the quantum information in a qubit by introducing redundancy into the physical system. Leghtas, Kirchmair, Vlastakis, *et al.* [4], Mirrahimi, Leghtas, Albert, *et al.* [5] propose and Ofek, Petrenko, Heeres, *et al.* [6] demonstrate a method to encode the quantum information in a clever basis in quantum harmonic resonators.

To further clarify, in this scheme the quantum information of a qubit is carefully encoded and decoded into a resonator by applying optimized microwave pulses to the qubit and resonator system which will realise state transfers in both these systems. This thesis will focus on how to numerically optimize encoding and decoding pulses using Krotov's method [7], a gradient ascent based optimization algorithm available publicly as a ready-to-use Python package [8].

1.1 Purpose

The purpose of this thesis is to numerically optimize microwave pulses to transfer the quantum information in a qubit to a resonator. This will be done using the Krotov Python package [8].

1.2 Limitations of the thesis

In this thesis, the limitations will be the following:

- The quantum systems are assumed to be closed systems without any interaction with the environment.
- The step size in Krotov's method will be constant throughout the optimizations.
- Single optimization goal (although multiple simultaneous are possible).

2 Theory

In this chapter the theoretical concepts will be explained. However it is assumed that the reader has a basic understanding of quantum mechanics.

2.1 Superconducting resonators

Superconducting resonators are used in quantum computing both as the basis for qubits and as readout and control components. Although ideal resonators have equally spaced energy levels, in reality they are more or less anharmonic and the general Hamiltonian for a quantum anharmonic resonator is

$$\hat{H} = \omega_q \hat{a}^\dagger \hat{a} + \frac{\kappa_q}{2}(\hat{a}^\dagger)^2 \hat{a}^2 \tag{2.1}$$

where ω_q is the resonance frequency, κ_q is the anharmonic (self-Kerr) term and $\hat{a}$ is the destruction operator which removes an excitation from the resonator. Note that this is still an approximation as higher order terms have been neglected.

The anharmonicity can be vizualised, see fig. 2.1, by plotting the eigenenergies of eq. (2.1) as a function of κ. A larger anharmonicity makes the energy spacing larger for excitation states higher than $|1\rangle$. This anharmonicity is what permits a resonator to act as a qubit, as it is possible to adress only the first two states $|0\rangle$ and $|1\rangle$ due to the frequency difference. Throughout this thesis, the term "qubit" will be used to refer to an anharmonic resonator even though it has more than two energy levels. Further, the "resonance frequency of the qubit" which correspond to the energy spacing between the first two levels, will be referred to as ω_q.

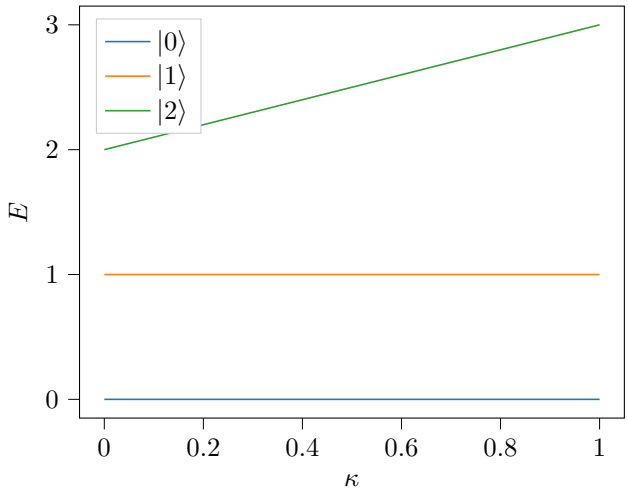

Figure 2.1: The energy levels of a three-level resonator for anharmonicity $\kappa \in [0, 1]$ and $\omega_q = 1$.

2.2 Coupled Qubit-Resonator System

The Hamiltonian for a coupled qubit and resonator is chosen as

$$\hat{H}(t) = \underbrace{\omega_r \hat{a}^\dagger \hat{a} + \frac{\kappa_r}{2}(\hat{a}^\dagger)^2 \hat{a}^2}_{\text{Resonator}} + \underbrace{\omega_q \hat{b}^\dagger \hat{b} + \frac{\kappa_q}{2}(\hat{b}^\dagger)^2 \hat{b}^2}_{\text{Qubit}} + \underbrace{g\left(\hat{a}^\dagger \hat{b} + \hat{a}\hat{b}^\dagger\right)}_{\text{Coupling}} \tag{2.2}$$

where $\hat{b}$ is the destruction operator for the qubit. There is now a coupling term with the coupling strength g which means that the resonator and the qubit can exchange excitations between each other. g will be assumed to be real for simplicity. This is similar to the Jaynes-Cummings Hamiltonian, but now there are added self-Kerr terms for both the qubit and the resonator. Another difference is that the Jaynes-Cummings model explicitly deals with a two-level qubit or atom, while this model has a "qubit" with arbitrary levels. Note that the rotating wave approximation has been applied to the coupling term [9].

2.3 Cat code

The cat code is a logical basis for quantum information stored in resonators. The basis states are

$$|0_L\rangle = |C_{\ \alpha}\rangle\,, \quad |1_L\rangle = |C_{i\alpha}\rangle \tag{2.3}$$

where

$$\left|C_{(i)\alpha}\right\rangle = \frac{1}{\sqrt{2}}(|(i)\alpha\rangle + |-(i)\alpha\rangle). \tag{2.4}$$

That is the each basis state $|0(1)_L\rangle$ in the cat code consists of a cat state $\left|C_{(i)\alpha}\right\rangle$, which is a superposition of a coherent state $|(i)\alpha\rangle$ and its negative counterpart $|-(i)\alpha\rangle$. A coherent state can be represented in the Fock basis as

$$|(i)\alpha\rangle = \mathrm{e}^{-\frac{|(i)\alpha|^2}{2}} \sum_{n=0}^{\infty} \frac{((i)\alpha)^n}{\sqrt{n!}} |n\rangle\,. \tag{2.5}$$

The basis can also be in an odd parity where the two coherent states are subtracted instead of added, however only the even parity basis will be used in this thesis. A more detailed review of the cat code can be found in the supplementary information of [6].

2.4 Visualization of quantum states

In order to understand the results presented later in this thesis, some visualization techniques of quantum states are shown and explained.

2.4.1 Bloch sphere

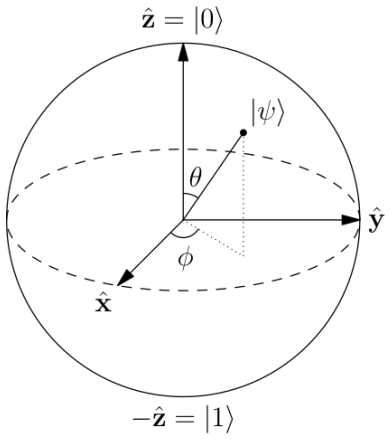

Figure 2.2: Representation of an abritrary pure quantum state on the Bloch sphere.
Source: [10] (CC BY-SA 3.0).

The pure state of a qubit can be visualized on the surface of a unit sphere with the following parametrization

$$|\psi\rangle = \cos\left(\frac{\theta}{2}\right)|0\rangle + \mathrm{e}^{i\phi}\sin\left(\frac{\theta}{2}\right)|1\rangle \tag{2.6}$$

where θ and ϕ are angles which are shown in fig. 2.2. The ground state $|0\rangle$ is located on the "north pole" and the excited state $|1\rangle$ on the "south pole".

Further, a handy trick to visualize the qubit when it has more levels than three is to "project" the state to the $\{|0\rangle, |1\rangle\}$ basis with $|0\rangle\langle 0| + |1\rangle\langle 1|$ and then plot it on the Bloch sphere. This means that the subspace which is not spanned by the first two levels will be represented by the inside of the sphere. To make an example, $|2\rangle$ will lie right in the center of the sphere while $(|1\rangle + |2\rangle)/\sqrt{2}$ will lie halfway between the center and the south pole.

2.4.2 Wigner function

The wigner function can be used to visualize quantum states and processes. It is a quasiprobability distribution where states exhibiting quantum phenomena will have negative values, impossible for classical states.

To give a visual example, 6 example states in the cat code basis are shown in fig. 2.3 with $\alpha = 2$ and a Hilber space size of $N = 8$. Looking at $|0\rangle$ we can see two lobes with an interference fringe in between them. For large enough N there will be no truncation of the Hilbert space and the lobes will appear circular. Compared to the basis states, the superposition states exhibit even more complex shapes.

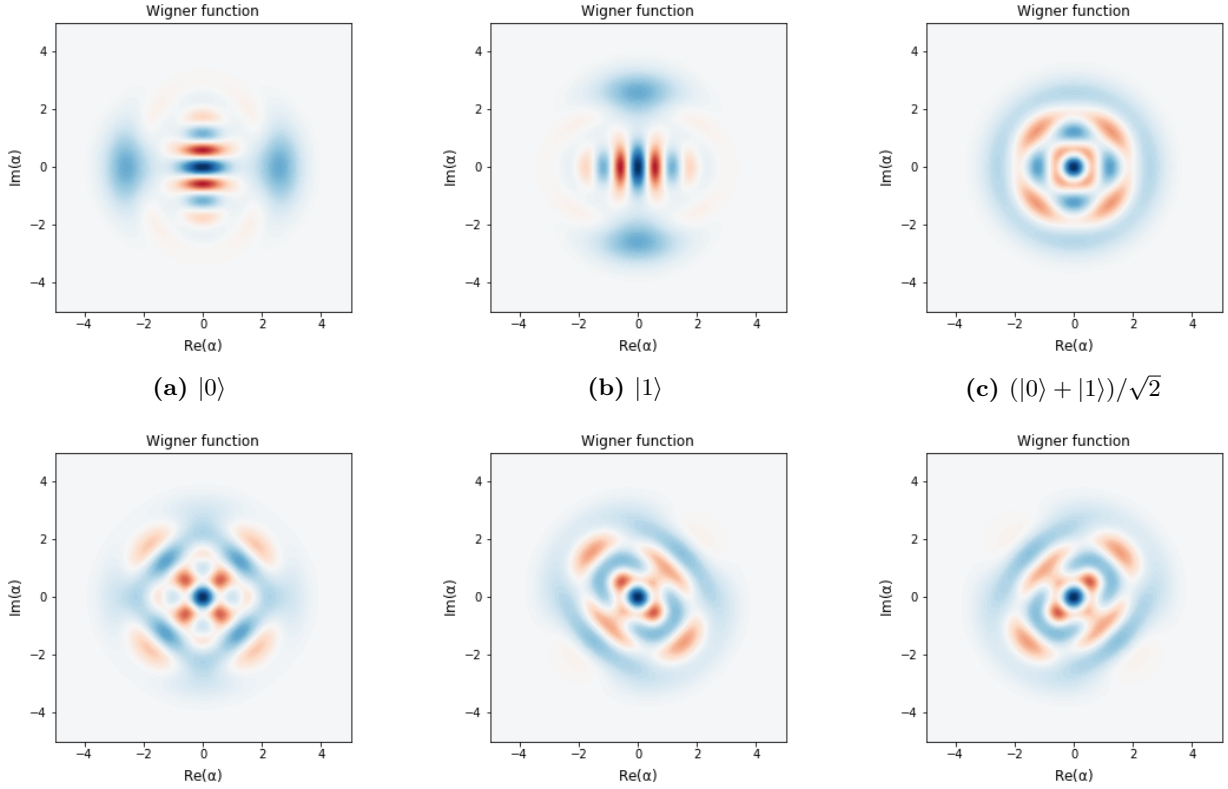

(a) $|0\rangle$ **(b)** $|1\rangle$ **(c)** $(|0\rangle + |1\rangle)/\sqrt{2}$

(d) $(|0\rangle - |1\rangle)/\sqrt{2}$ **(e)** $(|0\rangle + i\,|1\rangle)/\sqrt{2}$ **(f)** $(|0\rangle - i\,|1\rangle)/\sqrt{2}$

Figure 2.3: Wigner function of some example states in the cat code basis with $\alpha = 2$ and $N = 8$.

2.5 Quantum optimal control

Quantum control is the process of controlling a quantum system by controlling the amplitude of a set of control operators [11]. Such a system can be described [11] by a Hamiltonian of the following form

$$\hat{H}(t) = \underbrace{\hat{H}_d}_{\text{Drift}} + \underbrace{u_0(t)\hat{H}_0 + \ldots + u_N(t)\hat{H}_N}_{\text{Control}}. \tag{2.7}$$

The controls are usually electromagnetic pulses changing in time and thus will be referred to as "pulse shapes" [11] in this thesis .

There are two main questions in quantum control: one of *controllability* and one of *optimal control*. The first deals with the *existence* of solutions given a Hamiltonian and the second with the *optimized* solutions for the pulse shapes $\{u_i(t)\}$ [12]. The optimal solutions are generally not analytically solvable and thus the pulse shapes need to be discretized in time and numerically optimized using algorithms. The algorithm used for this thesis is called Krotov's method and will be presented in the Method chapter.

2.5.1 Unitary transformation

A unitary transformation can drastically simplify systems that are hard to simulate. This idea will be conceptually presented here and then implemented in the Method chapter. The transformation that is used is a special case of unitary transformations called the *interaction picture* where the Hamiltonian is split up into a time-independent and time-dependent part

$$\hat{H}(t) = \hat{H}_A + \hat{H}_B(t). \tag{2.8}$$

By choosing the unitary operator $\hat{U} = \mathrm{e}^{i\hat{H}_A t}$ the unitary transformation takes us into the interaction picture

$$\begin{aligned}
\hat{H} \rightarrow\ & \hat{U}\Big[\hat{H}_A + \hat{H}_B(t)\Big]\hat{U}^\dagger + i\frac{\mathrm{d}\hat{U}}{\mathrm{d}t}\hat{U}^\dagger = \\
=\ & \hat{U}\hat{H}_A\hat{U}^\dagger + \hat{U}\hat{H}_B\hat{U}^\dagger + i\Big(i\hat{H}_A t\Big)\mathrm{e}^{i\hat{H}_A t}\mathrm{e}^{-i\hat{H}_A t} = \\
=\ & \hat{H}_A + \hat{U}\hat{H}_B\hat{U}^\dagger - \hat{H}_A = \hat{U}\hat{H}_B\hat{U}^\dagger
\end{aligned}$$

3 Method

In this chapter Krotov's method for quantum optimal control will be briefly introduced and an implementation as a Python package. Then the numerical experiments will be explained.

3.1 Krotov's Method for quantum optimal control

Krotov's method fundamentally relies on the variational principle to minimize a functional

$$J\left[\left\{\left|\phi_k^{(i)}(t)\right\rangle\right\}, \left\{\epsilon_l^{(i)}(t)\right\}\right]$$

where constraints are included as Lagrange multipliers [8]. A detailed explanation of this functional when the method is applied to quantum systems can be found in [7]. However a quick summary of how the method works will be presented here. Starting with some guess pulse shapes, the initial state is forward propagated in time using a Hamiltonian of the same form as eq. (2.7) and the value of the functional is calculated. Then changes to the pulse shapes which will decrease the value of the functional are calculated, by propagating states with these new pulse shapes, and these updates become the new pulse shapes. This continues until convergence is reached.

The underlying mathematical principles of Krotov's method will not be adressed in the thesis, as that is outside the scope. Therefore the method will be treated as a black box function provided by the Python package which will be presented in the next section.

3.1.1 Krotov: the Python package

A Python implementation of the Krotov's method is available at [8] which provides an abstraction layer for doing optimizations. The package will be referred to as `krotov`. The reason `krotov` was chosen is primarily because it allows for optimization of multiple objectives simultaneously. This is necessary in order to create a single encoding pulse which will realise the state transfer into the cat code basis for any arbitrary state.

The package is built on top of QuTiP, a popular software package for simulating the dynamics of quantum systems [13]. That means it can leverage all the useful features of that package, which is also another reason this method was chosen. The package provides a set of submodules which are used to setup the optimization problem. The important modules will be presented here.

The `objectives` module describes the goal of the optimization, be it a state-to-state transfer or a quantum gate. It is used to specify the initial and target states, the Hamiltonian and the initial guess pulses.

The `functionals` module provides a set of functionals which can be used for Krotov's method. In this work the functional `chis_ss` has been chosen for all optimizations.

In the `convergence` module, help functions for the stopping criteria are provided for the optimization. It exposes values such as the overlap of the forward propagated state and target state $\langle\psi(T)|\psi_{\text{tar}}\rangle$ during the optimization which can be used to check when convergence is reached. The stopping criteria chosen for this thesis is either a minimum fidelity

$$F = \frac{1}{N}\sum_{k=1}^{N} |\langle\psi(T)|\psi_{\text{tar}}\rangle|^2, \tag{3.1}$$

where N is the number of (simultaneous) state transfers we want to realise, or when the change in fidelity between iterations ΔF falls below a specified value (a local minimum can be assumed to have been reached). The values of these will be specified in section 3.2

Finally, the `optimization` module is used to setup the whole optimization. It is possible to choose the time discretization, convergence criteria, optimization functional, and a function which will run after every iteration. Also the step size $1/\lambda$ of the pulse updates can be chosen which is further explained in [8]. Note however that although a large step size could achieve faster convergence, it can also lead to numerical instability.

3.2 Optimization Experiments

In this chapter the numerical optimization experiments are presented and motivated. The first experiment was used to assess the viability of the method, while the last one is a proof of concept for encoding states into the cat code basis.

3.2.1 Qubit state transfers

In this experiment, the optimization was run to realise the state transfer $|0\rangle \rightarrow |1\rangle$ and then $|0\rangle \rightarrow |2\rangle$. The first transfer should be close to the ideal solution of a π-pulse, while the second is non-trivial. Therefore they are suitable goals to test the method and package.

Hamiltonian

The anharmonic oscillator (qubit) in eq. (2.1) was chosen as it is a simple model for a physical qubit. As stated earlier such a system will be referred to as a qubit even though it has more than two energy levels. To induce transitions between the states of the qubit, control pulse terms were added to eq. (2.1)

$$\hat{H} = \omega_q \hat{a}^\dagger \hat{a} + \frac{\kappa}{2}\big(\hat{a}^\dagger \hat{a}\big)^2 + \Omega(t)\mathrm{e}^{-i\omega_q t}\hat{a} + \Omega^*(t)\mathrm{e}^{i\omega_q t}\hat{a}^\dagger \tag{3.2}$$

where $\Omega(t)$ is the complex amplitude of the control pulse. Looking at the Hamiltonian above it can be argued that it can be written in the form in eq. (2.7), which is needed by `krotov`, with $u_0(t) = \Omega(t)\mathrm{e}^{i\omega_q t}$ and $u_1(t) = \Omega^*(t)\mathrm{e}^{-i\omega_q t}$. However, there are two problems that need to be adressed. Firstly, the oscillating factors require an unnecessarily fine time discretization of the pulses. Secondly, the Krotov package expects real-valued pulse amplitudes $\{u_i(t)\}$ as inputs. The first problem was avoided by transforming the Hamiltonian into the interaction picture. Choosing $H_A = \omega_q \hat{a}^\dagger \hat{a}$, eq. (3.2) transforms[1] into

$$\hat{H} \rightarrow \ \frac{\kappa}{2}\big(\hat{a}^\dagger \hat{a}\big)^2 + \Omega(t)\hat{a} + \Omega^*(t)\hat{a}^\dagger. \tag{3.3}$$

Now the pulse amplitudes were $u_0(t) = \Omega(t)$ and $u_1(t) = \Omega^*(t)$, i.e. the envelope of the physical control pulse which varies significantly slower than the actual pulse. The second problem was easily fixed with a rearrangment of the terms

$$\begin{aligned}\Omega(t)\hat{a} + \Omega^*(t)\hat{a}^\dagger &= \Big[\mathrm{Re}[\Omega(t)] + i\mathrm{Im}[\Omega(t)]\Big]\hat{a} + \Big[\mathrm{Re}[\Omega(t)] - i\mathrm{Im}[\Omega(t)]\Big]\hat{a}^\dagger = \\ &= \mathrm{Re}[\Omega(t)]\big(\hat{a} + \hat{a}^\dagger\big) + \mathrm{Im}[\Omega(t)]i\big(\hat{a} - \hat{a}^\dagger\big).\end{aligned}$$

For intuition, $\big(\hat{a} + \hat{a}^\dagger\big)$ and $i\big(\hat{a} - \hat{a}^\dagger\big)$ correspond to Bloch sphere rotations around the x-axis and y-axis respectively. Thus the final Hamiltonian became

$$\hat{H} = \underbrace{\kappa/2\big(\hat{a}^\dagger \hat{a}\big)^2}_{\hat{H}_d} + \underbrace{\mathrm{Re}[\Omega(t)]}_{u_0(t)}\underbrace{\big(\hat{a} + \hat{a}^\dagger\big)}_{\hat{H}_0} + \underbrace{\mathrm{Im}[\Omega(t)]}_{u_1(t)}\underbrace{i\big(\hat{a} - \hat{a}^\dagger\big)}_{\hat{H}_1}. \tag{3.4}$$

The parameters of the qubit were chosen to model real superconducting qubits with $\kappa = -2\pi \times 297\,\mathrm{MHz}$ (and $\omega_q = 2\pi \times 6.2815\,\mathrm{GHz}$). The system Hamiltonian in eq. (3.4) was simulated with a Hilbert space size conveniently chosen to be $N_q = 3$. A smaller Hilbert space, and consequently smaller matrices, requires less computations but could possibly be a poor approximation of the Hamiltonian. Thus the solutions of the optimization were analysed with this in mind.

Optimization Setup

As the long-term goal is to use this method in physical systems some constraints were added. To simulate the constraints of physical **a**rbitrary **w**aveform **g**enerators a maximum sample rate of $4\,\mathrm{GSa\,s^{-1}}$ was chosen. Recall that the physcal pulses oscillate at $\omega_q = 6.2815\,\mathrm{GHz}$, a rate which $4\,\mathrm{GSa\,s^{-1}}$ can impossibly resolve. Although AWGs with higher sample rates than $4\,\mathrm{GSa\,s^{-1}}$ exist, they are expensive. However, rotating frame transformation permits the use of a relatively low rate AWG to generate the pulse envelopes $\Omega(t)$ and a high rate tone generator to create a carrier signal at ω_q, with these signals later combined in a mixer. Further, due to the noise sensitivity of superconducting systems an amplitude constraint is needed to keep the system cool enough. To set a realistic maximum amplitude A_m some derivation was required. First the maximum amplitude was chosen with the assumption that a gaussian pulse

$$g(t) = \frac{\pi/2}{\sigma\sqrt{2\pi}}\mathrm{e}^{-\frac{1}{2}\left(\frac{t}{\sigma}\right)^2} \tag{3.5}$$

[1] Full derivation is shown in **??**

with $\sigma = 3\,\text{ns}$ can physically realise a π-rotation $|0\rangle \to |1\rangle$ in a planar transmon qubit. The problem with gaussian pulses however is that they don't go to zero at the edges. To fix this `krotov` provides a function for generating Blackman pulses. A Blackman pulse with a total length of 6σ is a good approximation of a Gaussian pulse, with the added benefit of going to zero at the edges. However, due to the approximation, the integral of the Blackman pulse will not exactly be equal to the integral of the corresponding gaussian pulse, which is needed to realise the π-rotation. This can be fixed by using a prefactor C which can be calculated by solving

$$C \int_0^{6\sigma} \frac{1}{\sqrt{2\pi}\sigma} B(t) = \int_0^{6\sigma} g(t - 3\sigma)\,\mathrm{d}t \tag{3.6}$$

where $B(t)$ is the Blackman pulse. This is now used to determine the maximum amplitude

$$A(\sigma) = \frac{C}{\max(\sigma, 3)\sqrt{2\pi}} \tag{3.7}$$

with $A_m = A(\sigma = 3)$. This axmplitude constraint is enforced by calling a function after every iteration which limits all pulse shape values $|\Omega| < A_m$. Conveniently, the Blackman pulse was also used as the initial guess pulse with $u_0(t) = A(T/6)B(t)$.

Another constraint is that the edges of the pulses should always be zero with a switch-on/switch-off of 2 ns. This ramp shape is half a Blackman pulse and is provided by `krotov`'s `flattop` function.

For the $|0\rangle \to |1\rangle$ state transfer pulse shapes were optimized with varying lengths from 4.25 ns to 30 ns with convergence criteria $F > 0.99999$ or $\Delta F < 10^{-7}$. The step size was chosen as $\lambda = \frac{1}{\frac{1}{2}A_m}$. The reason for optimizing for various pulse lengths was that faster pulse changes gives a broader support in the frequency spectrum which can ultimately induce transitions in other levels. Therefore the optimization needs to find a solution which circumvents this problem.

Lastly, for the $|0\rangle \to |2\rangle$ state transfer pulse shapes were optimized with varying lengths from 22 ns to 30 ns with convergence criteria $F > 0.99999$ or $\Delta F < 10^{-9}$. The low ΔF was needed because the changes were very small in the beginning of the optimization. The step size was chosen as $\lambda = \frac{1}{2A_m}$ due to slow convergence. In contrast to the $|0\rangle \to |1\rangle$ state transfer both initial guess pulses were chosen to be Blackman pulses $u_0(t) = u_1(t) = A(T/6)B(T)$.

3.2.2 Cat code encoding

For the cat code encoding, 6 simultaneous objectives were chosen to give encoding pulses which maps the 6 furthest states on the Bloch sphere to the corresponding resonator states. These initial qubit states are (omitting normalization)

$$|0\rangle, |1\rangle,$$
$$|0\rangle + |1\rangle, |0\rangle - |1\rangle,$$
$$|0\rangle + i\,|1\rangle, |0\rangle - i\,|1\rangle$$

with target state $|0\rangle$, and the resonator initial state is $|0\rangle$ with target states

$$|C_{\ \alpha}\rangle, |C_{i\alpha}\rangle,$$
$$|C_{\ \alpha}\rangle + |C_{i\alpha}\rangle, |C_{\ \alpha}\rangle - |C_{i\alpha}\rangle,$$
$$|C_{\ \alpha}\rangle + i\,|C_{i\alpha}\rangle, |C_{\ \alpha}\rangle - i\,|C_{i\alpha}\rangle.$$

In summary the pulse shapes will realise the unitary

$$\hat{U}(T)(c_0\,|0\rangle + c_1\,|0\rangle) \otimes |0\rangle = |0\rangle \otimes (c_0\,|C_{\ \alpha}\rangle + c_1\,|C_{i\alpha}\rangle). \tag{3.8}$$

Hamiltonian

In this experiment the coupled qubit-resonator system in eq. (2.2) was used. As the operators $\hat{a}$ and $\hat{b}$ commute, eq. (3.4) was also used for the extra resonator. The rotating frame transformation is done with respect to $H_A = \omega_r \hat{a}^\dagger \hat{a} + \omega_q \hat{b}^\dagger \hat{b}$. However as the coupling term has no time dependence and does not commute with the operators there will still be a time dependence in the rotating frame

$$g(\hat{a}\hat{b}^\dagger + \hat{a}^\dagger \hat{b}) \to g(\hat{a}\hat{b}^\dagger \mathrm{e}^{i(\omega_q - \omega_r)t} + \hat{a}^\dagger \hat{b} \mathrm{e}^{-i(\omega_q - \omega_r)t}). \tag{3.9}$$

This was a problem because `krotov` expects $\hat{H}_d$ to be time independent. There is a way to "simulate" the coupling term by inserting it as an external time dependent pulse and omit it from optimization which was done in this case. The coupling term was then split into a real and imaginary part which is, as stated before, required by `krotov`.

The final Hamiltonian provided to `krotov` was then

$$\begin{aligned}\hat{H} = &\underbrace{\kappa_r/2\left(\hat{a}^\dagger\hat{a}\right)^2 + \kappa_q/2\left(\hat{b}^\dagger\hat{b}\right)^2}_{\hat{H}_d} + \\ &+ \underbrace{\mathrm{Re}[\Omega_r(t)]}_{u_0(t)}\underbrace{(\hat{a}+\hat{a}^\dagger)}_{\hat{H}_0} + \underbrace{\mathrm{Im}[\Omega_r(t)]}_{u_1(t)}\underbrace{i(\hat{a}-\hat{a}^\dagger)}_{\hat{H}_1} + \underbrace{\mathrm{Re}[\Omega_q(t)]}_{u_2(t)}\underbrace{(\hat{b}+\hat{b}^\dagger)}_{\hat{H}_2} + \underbrace{\mathrm{Im}[\Omega_q(t)]}_{u_3(t)}\underbrace{i(\hat{b}-\hat{b}^\dagger)}_{\hat{H}_3} + \\ &+ \underbrace{[\cos((\omega_q-\omega_r)t)]}_{u_4(t)}\underbrace{g(\hat{a}\hat{b}^\dagger+\hat{a}^\dagger\hat{b})}_{\hat{H}_4} + \underbrace{[\sin((\omega_q-\omega_r)t)]}_{u_5(t)}\underbrace{ig(\hat{a}\hat{b}^\dagger-\hat{a}^\dagger\hat{b})}_{\hat{H}_5}\end{aligned} \tag{3.10}$$

The parameters of this system is presented in table 3.1.

Table 3.1: Hamiltonian parameters

Param.	Value
$\omega_q/(2\pi)$	6.2815 GHz
$\kappa_q/(2\pi)$	297 MHz
$\omega_r/(2\pi)$	8.3056 GHz
$\kappa_r/(2\pi)$	4.5 kHz
$g/(2\pi)$	1.413 GHz

The Hilbert space size for the resonator was chosen to be $N_r = 8$ with the mean photon number $\alpha = 2$. Due to the large system size, the qubit Hilbert space size was set to $N_q = 2$.

Optimization setup

The optimization was setup in the same way as the previous experiment, however due to the rapid oscillations at $|\omega_q - \omega_r|$ a finer time discretization of $24\,\mathrm{GSa\,s^{-1}}$ was chosen. The step size was chosen as $\lambda = \frac{1}{\frac{1}{2}A_m}$ and the pulse length $T = 60\,\mathrm{ns}$ to allow the coupling to affect the system. Further, convergence criteria was chosen as $F > 0.999999$ or $\Delta F < 10^{-6}$. Another important step in optimizing in the rotating frame was to convert the target states into the rotating frame by multiplying with $U^\dagger = \mathrm{e}^{i\hat{H}_A T}$. This was needed for the final states to be the correct ones in the lab frame. Initial guess pulses were chosen to be a Blackman pulse corresponding to a π-rotation of the qubit in the previous experiment.

4 Results

The results of the numerical experiments will be presented in this chapter. For both optimization targets the optimized pulses, their properties and the final evolved state will be presented.

4.1 Qubit state transfers

4.1.1 $|0\rangle \rightarrow |1\rangle$ state transfer

In fig. 4.1 the fidelity during all optimization runs are plotted. For pulse lengths longer than 15 ns the fidelity starts at values close to the goal ($F > 0.9$) and the number of iterations is relatively low (less than 85 iterations). In contrast, pulses shorter than 15 ns start at lower fidelities while the number of iterations are roughly one order of magnitude larger with no clear pattern with respect to the pulse length.

To give a more detailed picture, the starting fidelity and optimized fidelity is plotted over pulse length in fig. 4.2. The optimizations where the fidelity goal was not reached, pulse lengths equal to and below 10.50 ns, are marked with stars.

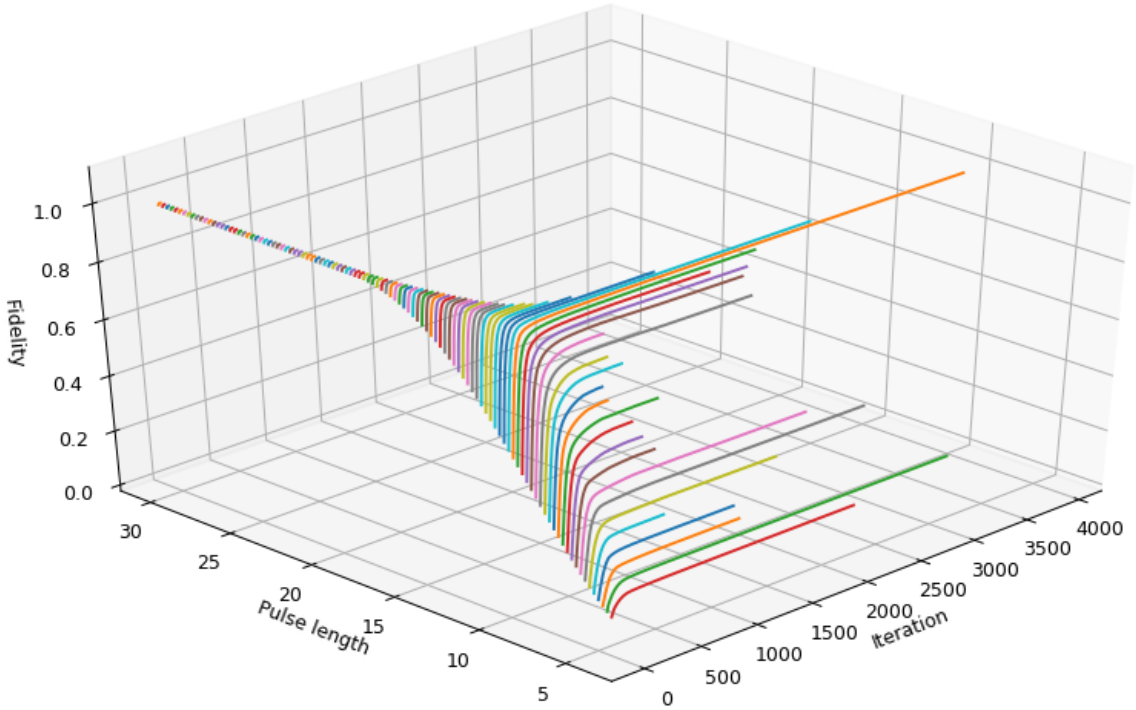

Figure 4.1: Fidelity during optimizations for every pulse length (ns). The different colors help distinguish the lines.

Further analysis is done on pulses with lengths 4.25 ns, 6.0 ns, 8.0 ns, 10.0 ns, 20.0 ns and 30.0 ns. The optimized pulse shapes $\mathrm{Re}(\Omega)$ and $\mathrm{Im}(\Omega)$ are plotted in fig. 4.3 together with the guess pulses. Pulses longer than 20 ns require only fine adjustments to the Blackman guess pulse while shorter pulses have an imaginary part which is maximized for the whole duration of the pulse.

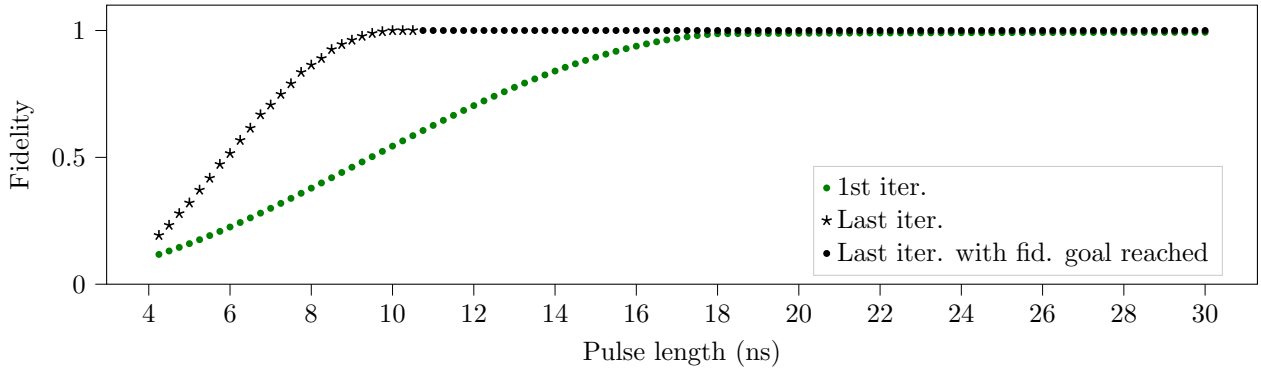

Figure 4.2: Fidelity of first and last iteration of every pulse length.

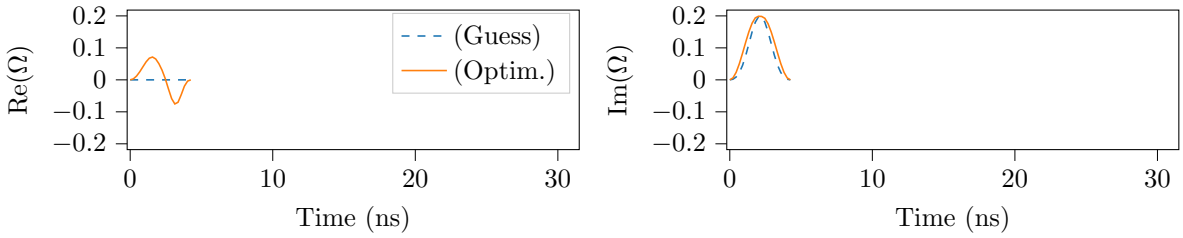

(a) Pulse length 4.25 ns

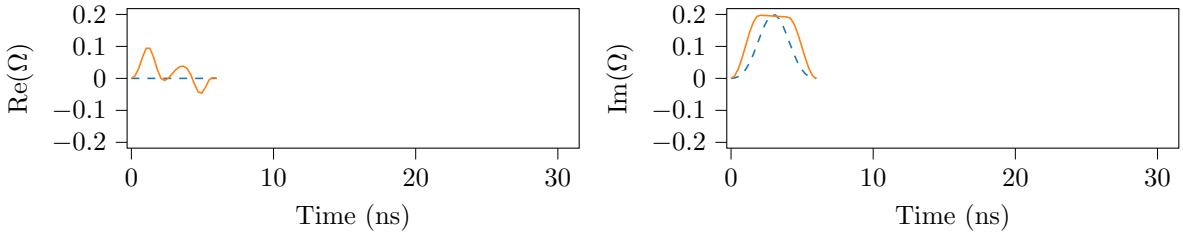

(b) Pulse length 6.0 ns

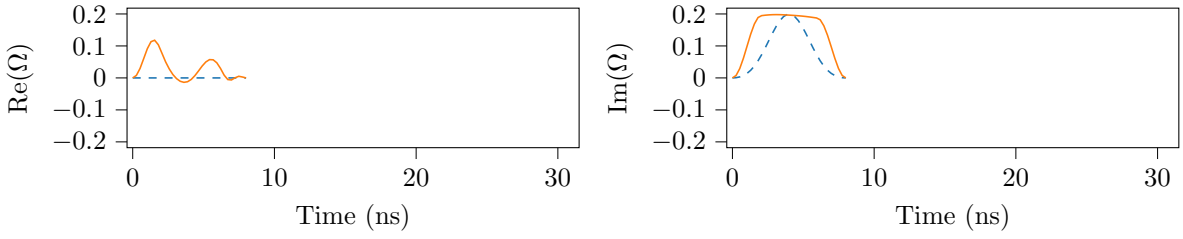

(c) Pulse length 8.0 ns

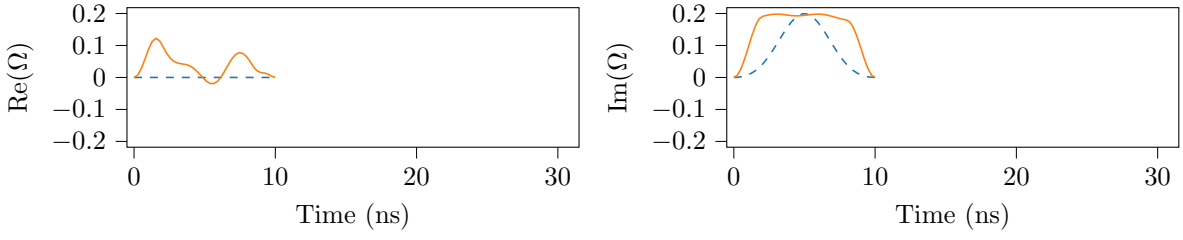

(d) Pulse length 10.0 ns

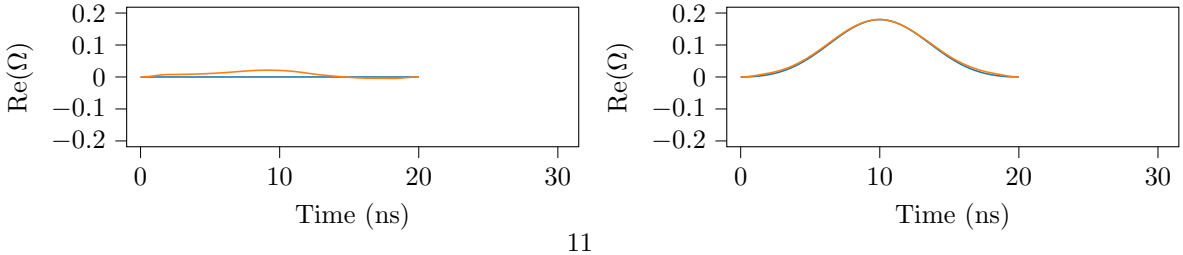

(e) Pulse length 20.0 ns

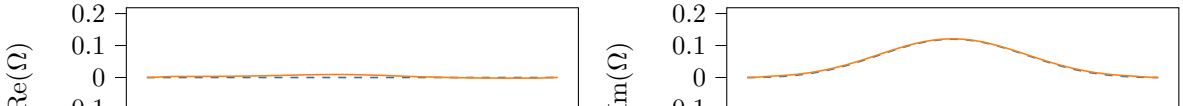

The spectrum of $\Omega(t)$ in the lab frame ($\Omega(t)e^{i\omega_q t}$) is shown in fig. 4.4. For all pulse lengths there is a peak centered roughly at ω_q with a quickly decaying end in positive direction (towards $\omega_q + \kappa_q$). Following the trend, it can be observed that the width of the peak becomes narrower for longer pulses. For the highest pulse length 30 ns there is almost no support at $\omega_q + \kappa_q$ nor $\omega_q - \kappa_q$.

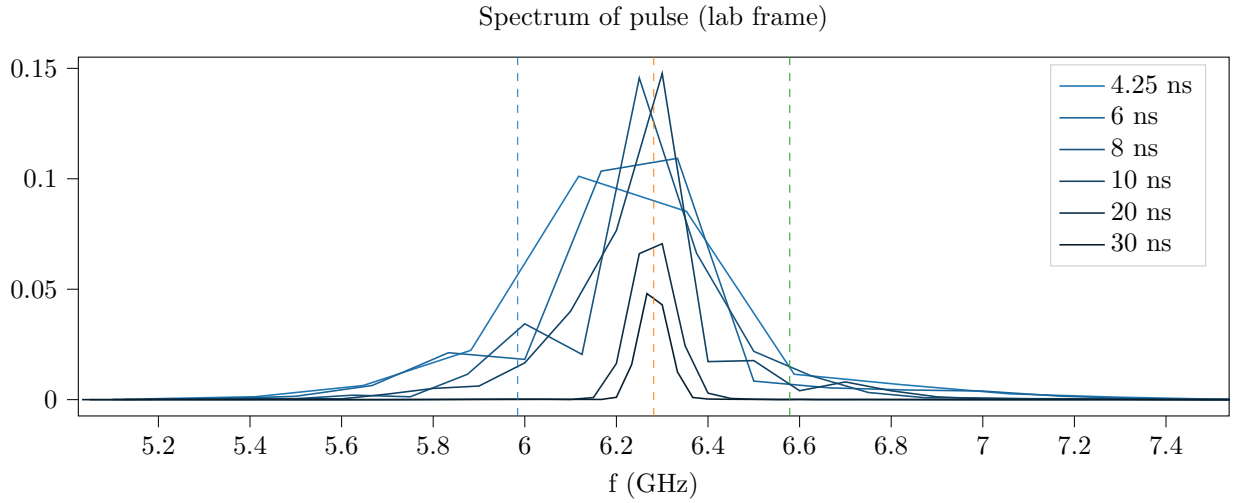

Figure 4.4: Frequency spectrum of the complex pulses in fig. 4.3. The vertical lines indicate (from left to right) $\omega_q - \kappa_q$, ω_q, $\omega_q + \kappa_q$ (all divided by 2π).

The time evolution of the system under the optimized pulses are visualized by plotting the occupation of the states over time, fig. 4.5, and the projection of the state on the Bloch sphere over time, fig. 4.6.

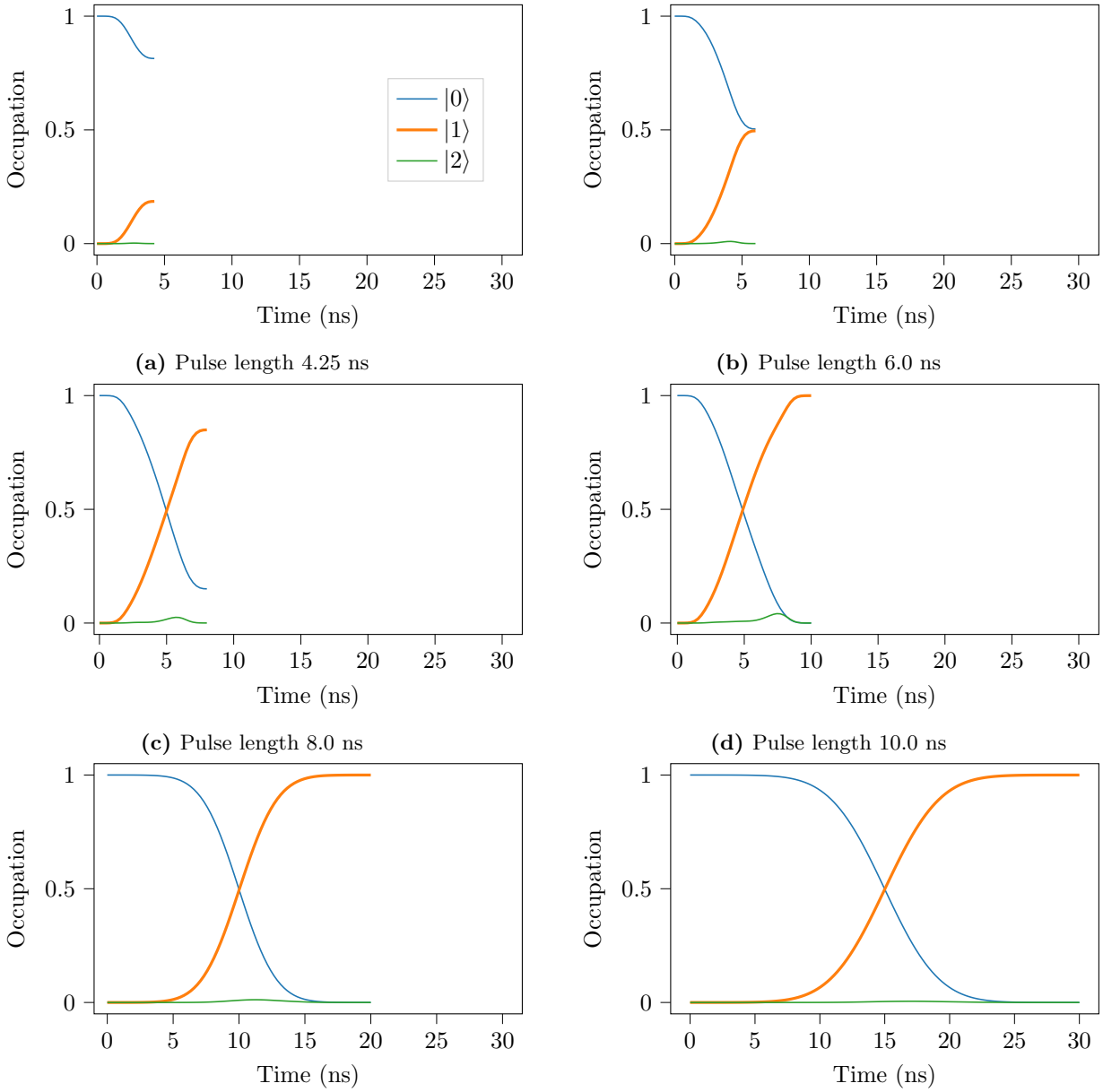

(a) Pulse length 4.25 ns

(b) Pulse length 6.0 ns

(c) Pulse length 8.0 ns

(d) Pulse length 10.0 ns

(e) Pulse length 20.0 ns

(f) Pulse length 30.0 ns

Figure 4.5: Energy level occupation over time for different lengths of optimized pulses.

For short pulse lengths there is not enough time for the transfer from $|0\rangle$ to $|1\rangle$, but for a pulse length of roughly 10.0 ns the goal is reached. Figure 4.5 **(b)** shows a little rise in occupation of $|2\rangle$ around 7.5 ns.

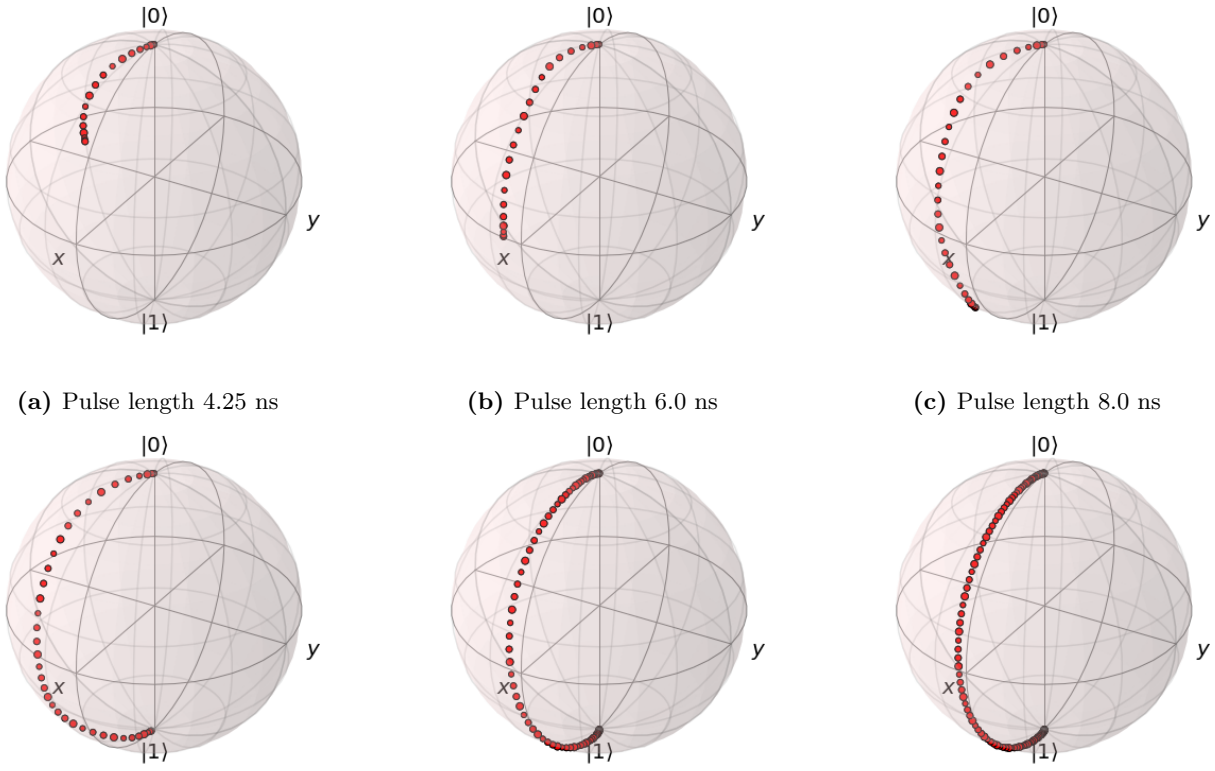

(a) Pulse length 4.25 ns **(b)** Pulse length 6.0 ns **(c)** Pulse length 8.0 ns

(d) Pulse length 10.0 ns **(e)** Pulse length 20.0 ns **(f)** Pulse length 30.0 ns

Figure 4.6: Time dynamics on the Bloch sphere for different lengths of optimized pulses.

From the Bloch sphere visualization it appears that shorter pulse lengths lead to deviations from the pure y-axis rotation. This can be clearly seen in fig. 4.6 **(d)** for a pulse length of 10 ns, where the fidelity goal was reached but short enough that the maximum amplitude is reached for the guess pulse.

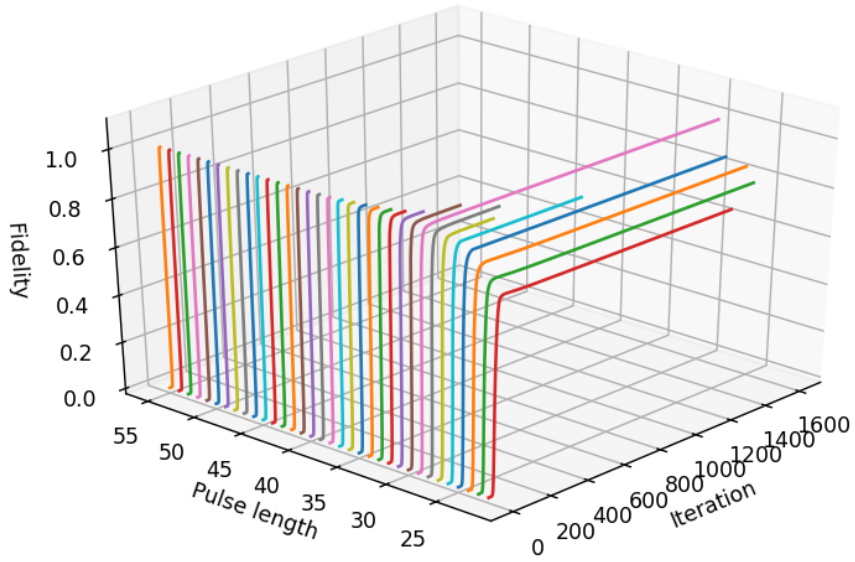

Figure 4.7: Fidelity during optimizations for every pulse length (ns).

4.1.2 $|0\rangle \rightarrow |2\rangle$ state transfer

Once again all optimization runs are shown in fig. 4.7. All runs start at almost zero fidelity while pulse lengths from 30 ns and up reach the fidelity goal of $F > 0.99999$. The number of iterations are relatively low down to 30 ns and for shorter pulses the iterations fluctuate. Note that for pulse lengths shorter than 22 ns the optimization stopped after the first iteration due to $\Delta F < 10^{-9}$.

In fig. 4.8 the fidelity is shown with respect to pulse length and here it is seen that the fidelity goal is reached for pulses down to 30 ns.

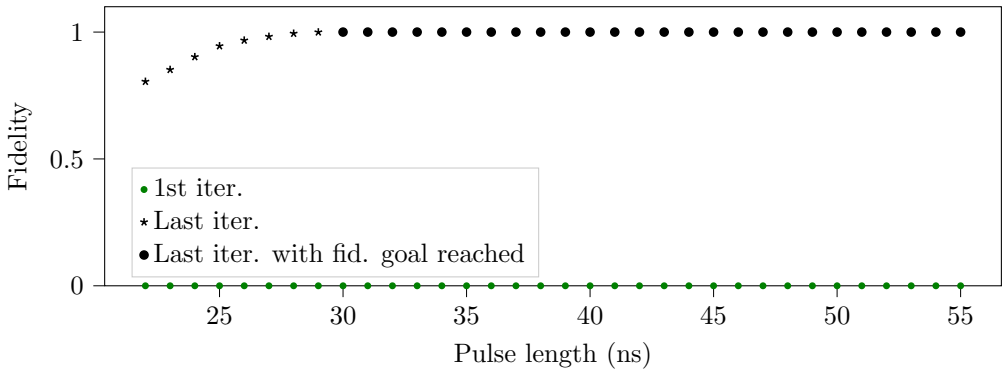

Figure 4.8: Fidelity of first and last iteration of every pulse length.

The optimized pulses are shown in fig. 4.9. For all pulse lengths the pulses have roughly the same shape with a quick rise and a short plateau, then oscillations until the end. The longest pulse at 55 ns has more oscillations than, but instead they are lower in amplitude. To get some insight, the frequency spectrum, fig. 4.10, shows large support at ω_q and $\omega_q + \kappa_q$, while for longer pulses a peak at $\omega_q - \kappa_q$ disappears. Just as the previous state transfer, the peaks narrow for longer pulse lengths.

The occupation dynamics in fig. 4.11 show a slow oscillation in all pulse lengths for all states. Further, the occupation probability of $|1\rangle$ rises to about 0.75 until the middle-point of the pulse and then falls to zero in the end, while $|2\rangle$ starts to rise at the point of the population inversion. For the shorter pulse lengths it can be seen that there isn't enough time to realise the transfer.

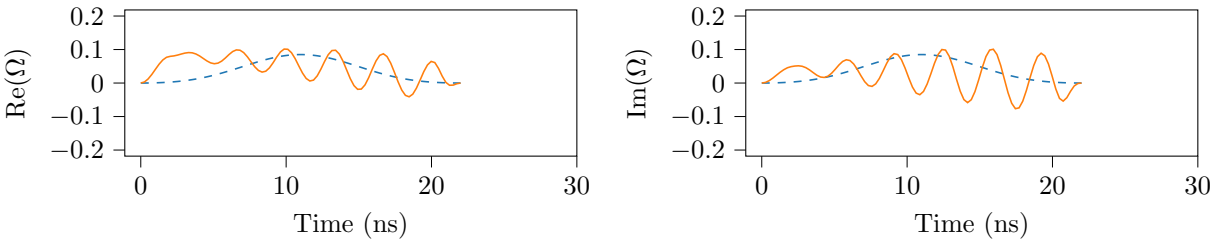

(a) Pulse length 22.0 ns

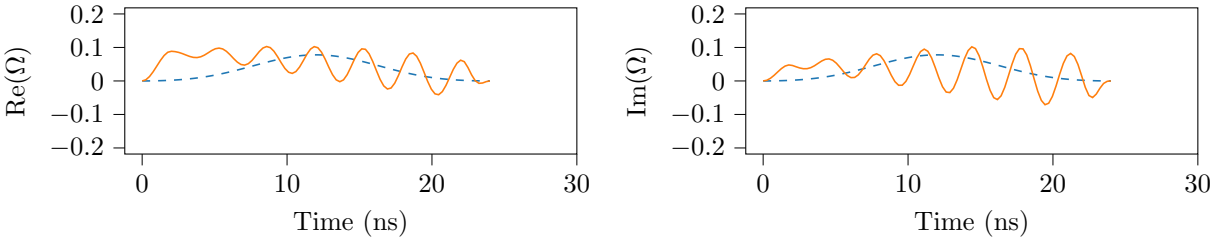

(b) Pulse length 24.0 ns

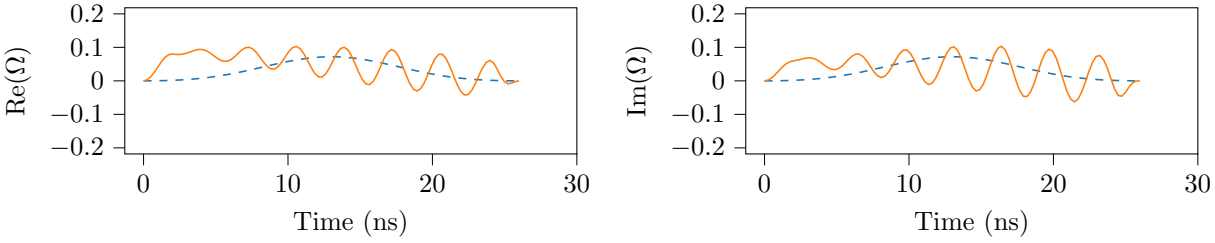

(c) Pulse length 26.0 ns

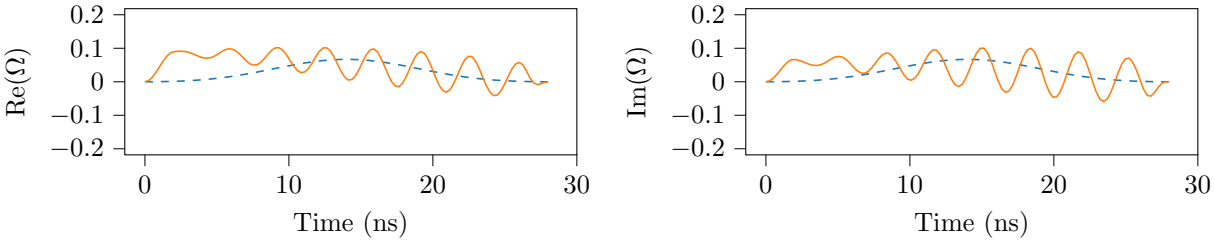

(d) Pulse length 28.0 ns

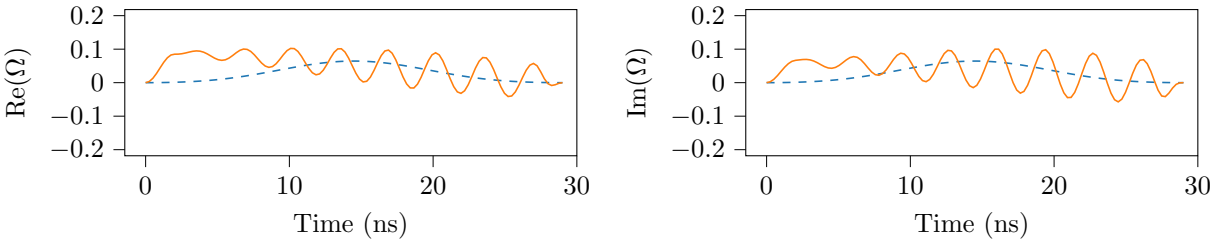

(e) Pulse length 29.0 ns

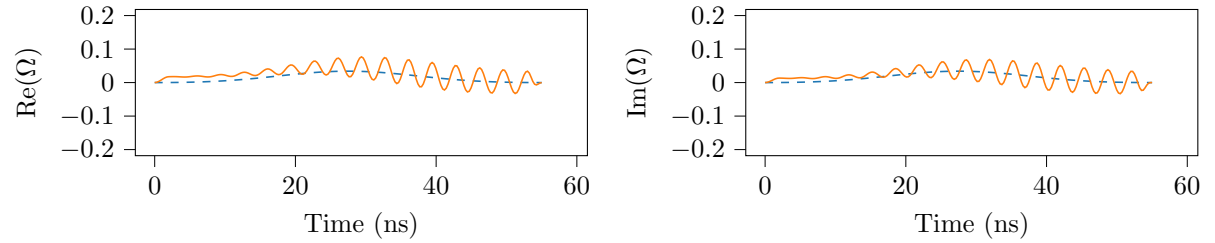

(f) Pulse length 55.0 ns

Figure 4.9: Optimised pulse shapes and guess pulses for pulse lengths **(a)** 22 ns, **(b)** 24 ns, **(c)** 26 ns, **(d)** 28 ns, **(e)** 29 ns, and **(f)** 55 ns. Oscillations appear in all solutions.

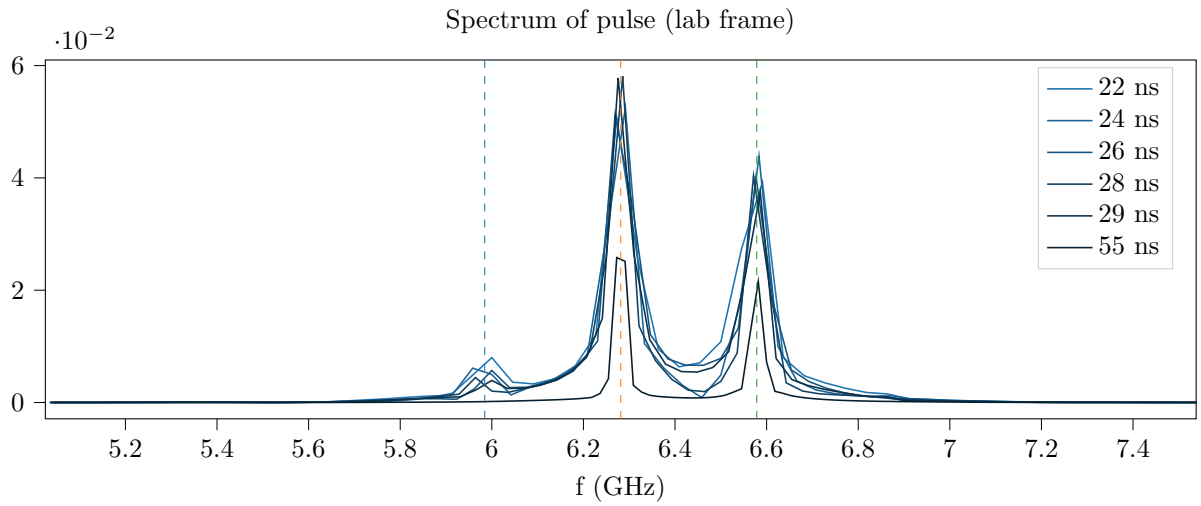

Figure 4.10: Frequency spectrum of the complex pulses in fig. 4.9. The vertical lines indicate (from left to right) $\omega_q - \kappa_q$, ω_q, $\omega_q + \kappa_q$ (all divided by 2π).

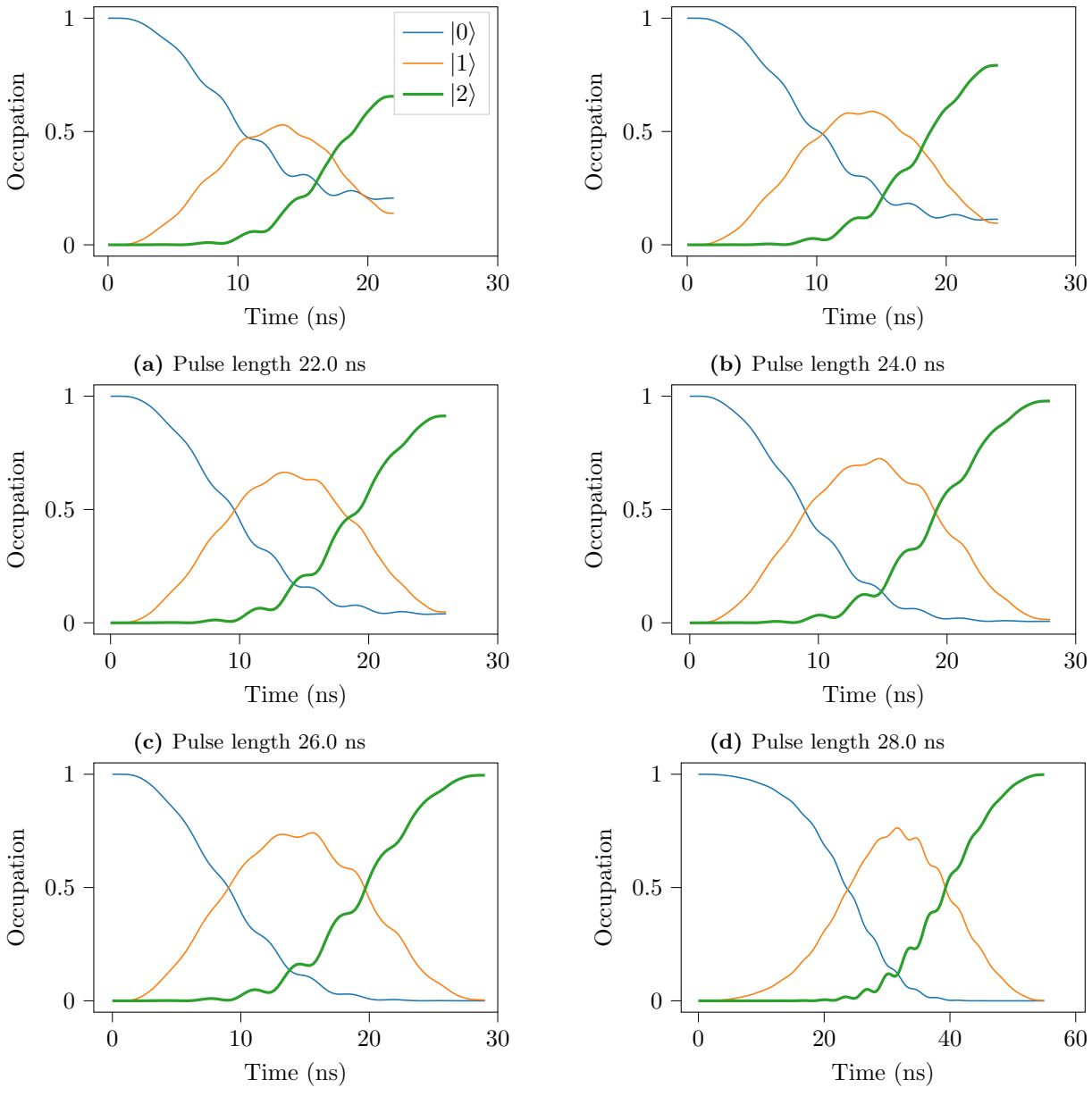

(a) Pulse length 22.0 ns

(b) Pulse length 24.0 ns

(c) Pulse length 26.0 ns

(d) Pulse length 28.0 ns

(e) Pulse length 29.0 ns

(f) Pulse length 55.0 ns

Figure 4.11: Energy level occupation over time for different lengths of optimized pulses.

4.2 Cat code encoding

The cat encoding optimization reached the convergence criteria of $\Delta F < 10^{-6}$ after 2389 iterations (totalling at roughly 41 hours and 28 minutes) with a fidelity $F = 0.999380$, recall the fidelity measure in eq. (3.1). The individual fidelities for the 6 initial states are shown in table 4.1, where we can see that all individual fidelities are above 0.999000.

Table 4.1: Fidelities for the individual state transfers (ordered from highest to lowest).

State	F
$(\|0\rangle - \|1\rangle)/\sqrt{2}$	0.999553
$(\|0\rangle + i\,\|1\rangle)/\sqrt{2}$	0.999411
$(\|0\rangle + \|1\rangle)/\sqrt{2}$	0.999363
$\|0\rangle$	0.999362
$\|1\rangle$	0.999320
$(\|0\rangle - i\,\|1\rangle)/\sqrt{2}$	0.999272

The pulse shapes of the qubit and resonator are shown in fig. 4.12. Comparing the resonator and qubit we can see that the resonator pulse has rapid oscillations throughout the whole pulse while the qubit exhibits some small quick oscillation at sparse times. The spectrum of the pulse is shown in **??** and gives us some insight into the pulse shapes. The qubit control pulse shows a wide peak at ω_q, two small peaks at ω_r and $2\omega_r - \omega_q$ and two barely noticable peaks at $\frac{1}{4}\omega_r$ and $\frac{1}{2}\omega_r$. The resonator pulse has one wide peak at ω_r, a smaller one at ω_q and an even smaller peak at $2\omega_r - \omega_q$.

The dynamics of the qubit is shown in fig. 4.14 for all state transfers. Here we see that there is always a rapid oscillation present in the occupation probability. Looking at the dynamical behaviour one can see that common for all transfers is for the qubit to stay somewhat close to an equal superposition between $|0\rangle$ and $|1\rangle$ and then at circa 50 ns evolve to $|0\rangle$.

The dynamics of the resonator are shown in **??** as there are too many states for one plot, however one interesting measure we can look at is the maximum occupation of the 8 resonator states. This can give us information about the the validity of the Hilbert space truncation. In fig. 4.15 the maximum reached occupation probability are plotted for all states. This is done for all the 6 state transfers. Looking only at the odd states there is a clear downward trend for higher states, with $|7\rangle$ only reaching circa 0.2 of occupation probability during the $|0\rangle$ transfer. $|6\rangle$ is in the 0.2–0.3 occupation range for all transfers.

Finally we can plot the Wigner function of the final resonator states and compare it with the target states. This is done in fig. 4.16 where the final states have been transformed back into the lab frame. As is evident from the plots they are close to the target states shown in fig. 2.3.

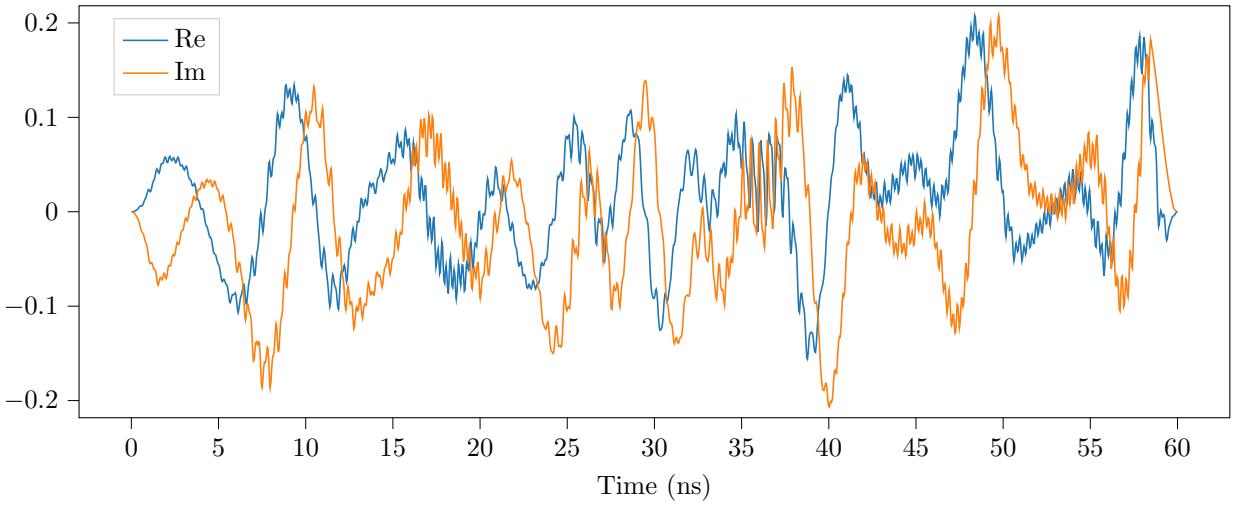

(a) Qubit control pulse shape.

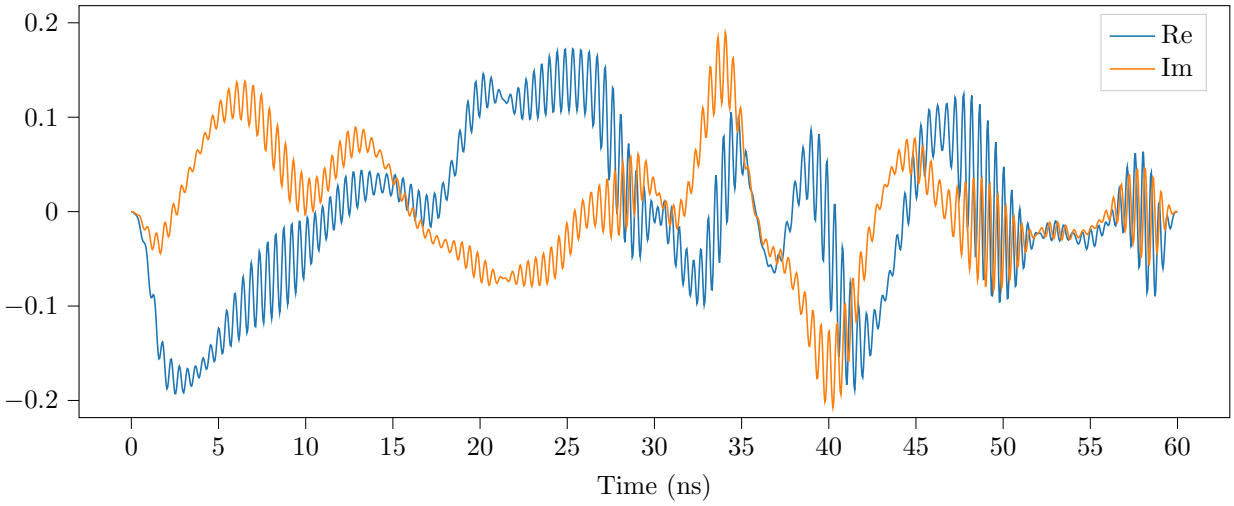

(b) Resonator control pulse shape.

Figure 4.12: Optimized pulse shapes of **(a)** $\Omega_q(t)$ and **(b)** $\Omega_r(t)$. The real and imaginary parts of the pulse are shown in blue and orange respectively. The resonator shows rapid oscillations compared to the qubit.

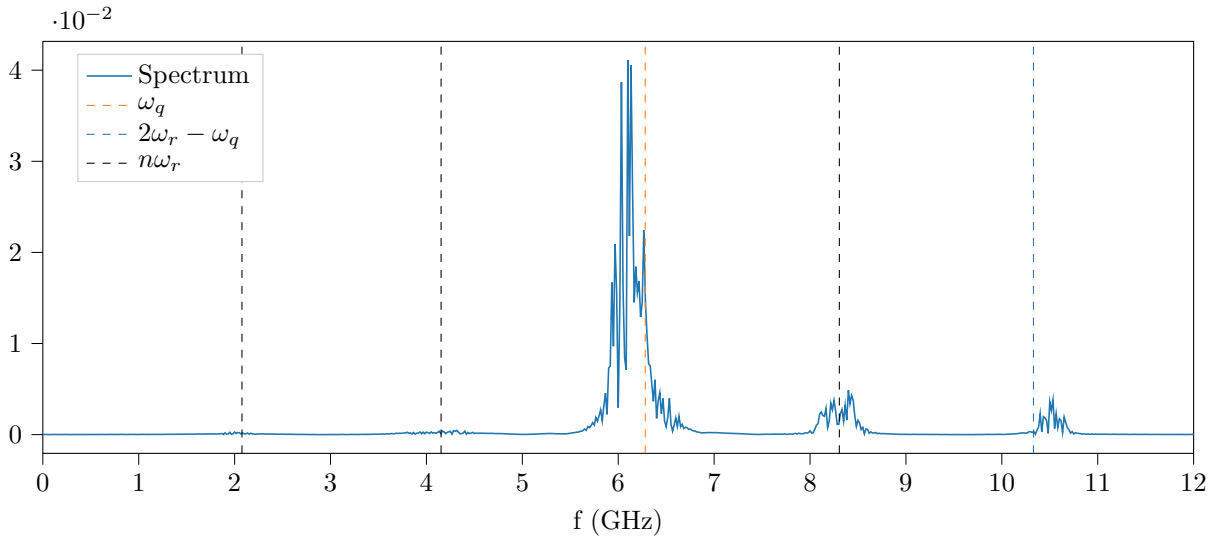

(a) Qubit control pulse spectrum. The black vertical are located at $n\omega_r$ where $n = (0.25, 0.5, 1)$.

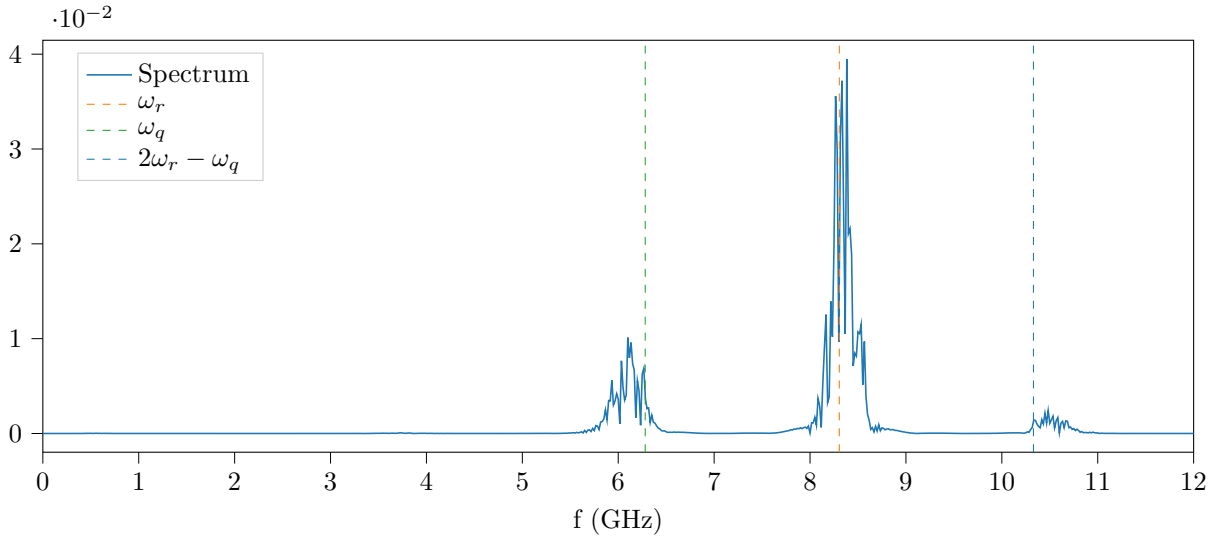

(b) Resonator control pulse spectrum.

Figure 4.13: Spectrum of optimized pulses **(a)** $\Omega_q(t)$ and **(b)** $\Omega_r(t)$ (in the lab frame).

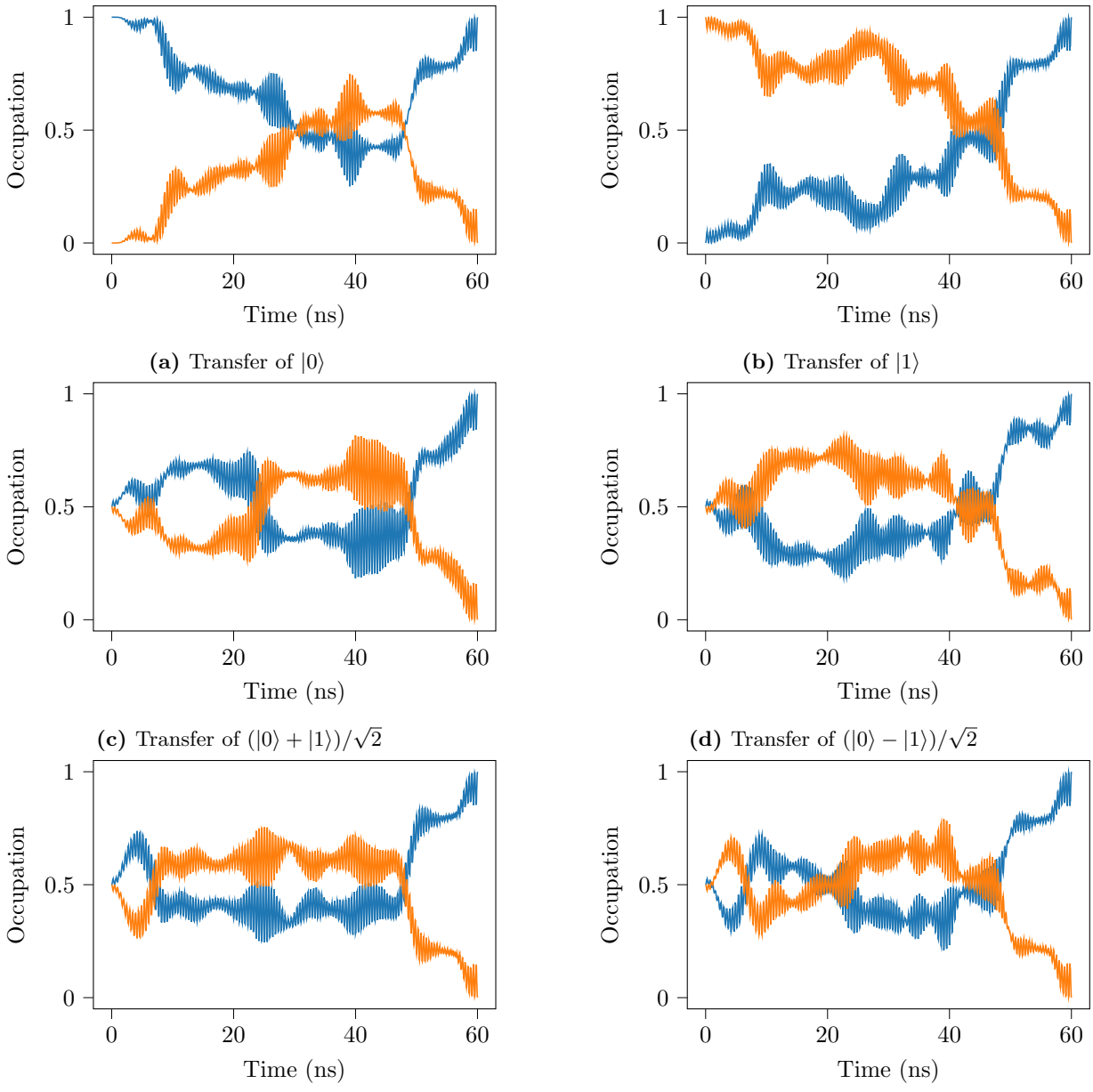

(a) Transfer of $|0\rangle$

(b) Transfer of $|1\rangle$

(c) Transfer of $(|0\rangle + |1\rangle)/\sqrt{2}$

(d) Transfer of $(|0\rangle - |1\rangle)/\sqrt{2}$

(e) Transfer of $(|0\rangle + i\,|1\rangle)/\sqrt{2}$

(f) Transfer of $(|0\rangle - i\,|1\rangle)/\sqrt{2}$

Figure 4.14: Qubit level occupation over time for the 6 state transfers. $|0\rangle$ and $|1\rangle$ are shown in blue and orange respectively.

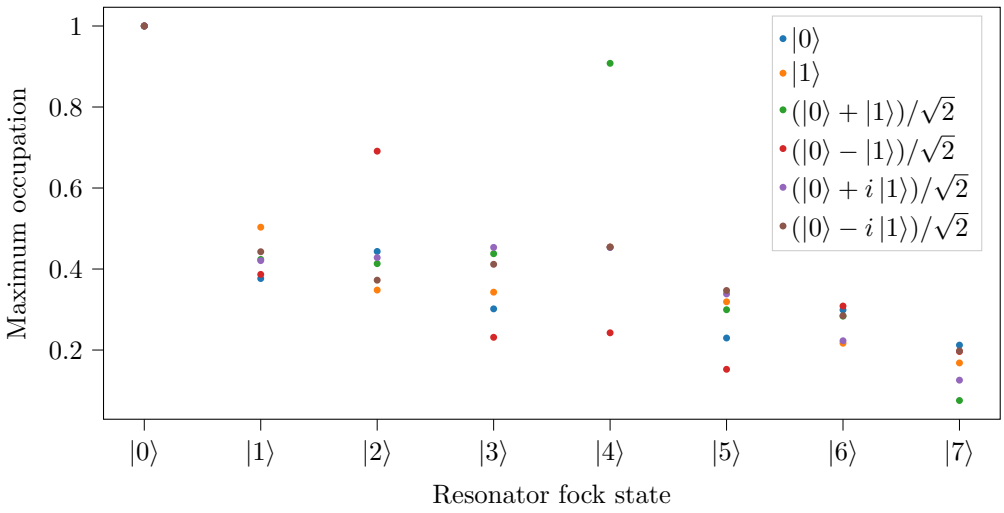

Figure 4.15: asda

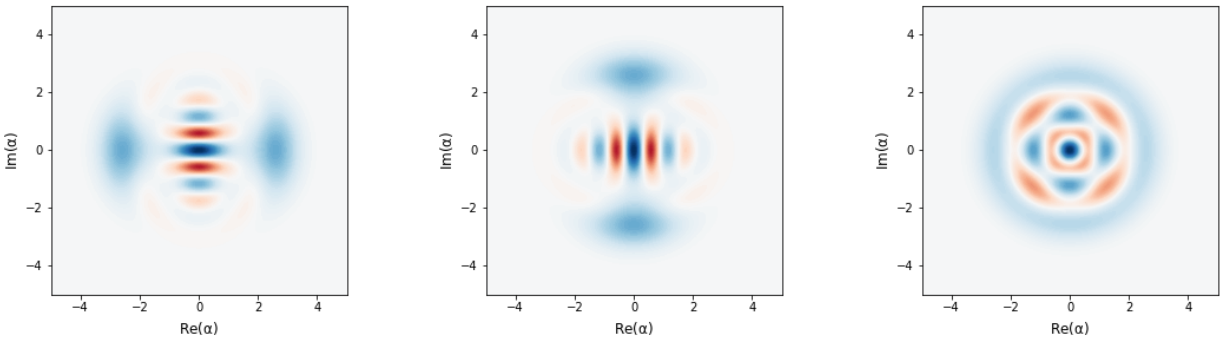

(a) Transfer of $|0\rangle$ **(b)** Transfer of $|1\rangle$ **(c)** Transfer of $(|0\rangle + |1\rangle)/\sqrt{2}$

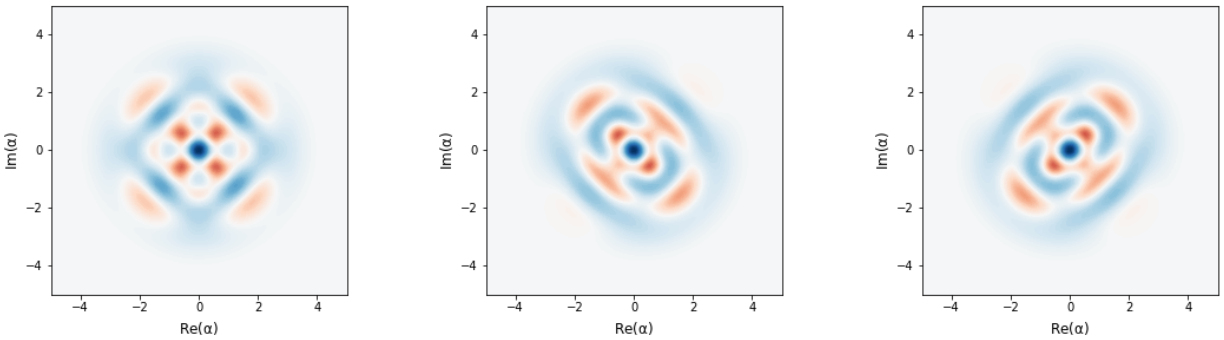

(d) Transfer of $(|0\rangle - |1\rangle)/\sqrt{2}$ **(e)** Transfer of $(|0\rangle + i\,|1\rangle)/\sqrt{2}$ **(f)** Transfer of $(|0\rangle - i\,|1\rangle)/\sqrt{2}$

Figure 4.16: Wigner function of final state (lab frame) of the resonator for all state transfers. The final resonator states are close to the target states shown in fig. 2.3.

5 Discussion

excpeted oscillations in pulse shapes for gf Finally, it is possible to relate the dynamics to the pulse shape. The small plateau drives the population inversion for

5.1 Cat code encoding

qubit oscillations are not stable at such a high coupling therefore final fidelity is not that robust

Reason to believe that 4 levels could be enough for the qubit

6 Conclusion

6.1 Future work

Dispersive regime Penalize higher states Include dissipation (Liouvillian) Ensemble optimization for different phases of the coupling pulses

References

[1] A. C. Santos, The IBM Quantum Computer and the IBM Quantum Experience, *Revista Brasileira de Ensino de Física* **39**, no. 1 Sep. 2016, Sep. 2016. DOI: 10.1590/1806-9126-RBEF-2016-0155. [Online]. Available: http://arxiv.org/abs/1610.06980 (visited on 05/10/2019).

[2] J. Preskill, Quantum Computing in the NISQ era and beyond, *Quantum* **2** Aug. 2018, 79, Aug. 2018. DOI: 10.22331/q-2018-08-06-79. [Online]. Available: http://arxiv.org/abs/1801.00862 (visited on 02/28/2019).

[3] D. Gottesman, An Introduction to Quantum Error Correction and Fault-Tolerant Quantum Computation, *arXiv:0904.2557 [quant-ph]* Apr. 2009, Apr. 2009. [Online]. Available: http://arxiv.org/abs/0904.2557 (visited on 05/10/2019).

[4] Z. Leghtas, G. Kirchmair, B. Vlastakis, R. J. Schoelkopf, M. H. Devoret, and M. Mirrahimi, Hardware-Efficient Autonomous Quantum Memory Protection, *Physical Review Letters* **111**, no. 12 Sep. 2013, 120501, Sep. 2013. DOI: 10.1103/PhysRevLett.111.120501. [Online]. Available: https://link.aps.org/doi/10.1103/PhysRevLett.111.120501 (visited on 05/10/2019).

[5] M. Mirrahimi, Z. Leghtas, V. V. Albert, S. Touzard, R. J. Schoelkopf, L. Jiang, and M. H. Devoret, Dynamically protected cat-qubits: A new paradigm for universal quantum computation, *New Journal of Physics* **16**, no. 4 Apr. 2014, 045014, Apr. 2014. DOI: 10.1088/1367-2630/16/4/045014. [Online]. Available: http://arxiv.org/abs/1312.2017 (visited on 01/29/2019).

[6] N. Ofek, A. Petrenko, R. Heeres, P. Reinhold, Z. Leghtas, B. Vlastakis, Y. Liu, L. Frunzio, S. M. Girvin, L. Jiang, M. Mirrahimi, M. H. Devoret, and R. J. Schoelkopf, Extending the lifetime of a quantum bit with error correction in superconducting circuits, English, *Nature; London* **536**, no. 7617 Aug. 2016, 441–445, Aug. 2016. DOI: http://dx.doi.org.proxy.lib.chalmers.se/10.1038/nature18949. [Online]. Available: http://search.proquest.com/docview/1815378608/abstract/D91F00AED7CC42E9PQ/1 (visited on 01/23/2019).

[7] D. M. Reich, M. Ndong, and C. P. Koch, Monotonically convergent optimization in quantum control using Krotov's method, *The Journal of Chemical Physics* **136**, no. 10 Mar. 2012, 104103, Mar. 2012. DOI: 10.1063/1.3691827. [Online]. Available: https://aip.scitation.org/doi/10.1063/1.3691827 (visited on 04/29/2019).

[8] M. H. Goerz, D. Basilewitsch, F. Gago-Encinas, M. G. Krauss, K. P. Horn, D. M. Reich, and C. P. Koch, Krotov: A Python implementation of Krotov's method for quantum optimal control, *arXiv:1902.11284 [quant-ph]* Feb. 2019, Feb. 2019. [Online]. Available: http://arxiv.org/abs/1902.11284 (visited on 03/13/2019).

[9] Y. Wu and X. Yang, Strong-Coupling Theory of Periodically Driven Two-Level Systems, *Physical Review Letters* **98**, no. 1 Jan. 2007, 013601, Jan. 2007. DOI: 10.1103/PhysRevLett.98.013601. [Online]. Available: https://link.aps.org/doi/10.1103/PhysRevLett.98.013601 (visited on 05/29/2019).

[10] Glosser.ca, *English: Bloch sphere; a geometrical representation of a two-level quantum system. Rendered with Asymptote.* Dec. 2012. [Online]. Available: https://commons.wikimedia.org/wiki/File:Bloch_Sphere.svg (visited on 05/22/2019).

[11] R. Fisher, "Optimal Control of Multi-Level Quantum Systems", Dissertation, Technische Universität München, München, 2010.

[12] D. d'Alessandro, *Introduction to quantum control and dynamics*. Chapman and Hall/CRC, 2007.

[13] J. R. Johansson, P. D. Nation, and F. Nori, QuTiP 2: A Python framework for the dynamics of open quantum systems, *Computer Physics Communications* **184**, no. 4 Apr. 2013, 1234–1240, Apr. 2013. DOI: 10.1016/j.cpc.2012.11.019. [Online]. Available: http://arxiv.org/abs/1211.6518 (visited on 05/28/2019).

A Appendix

A.1 Jupyter Notebooks and Optimization Data

To ease reproducibility the Jupyter notebooks and majority of data are available at `https://github.com/JohanWinther/cat-state-encoding`.

A.2 Cat code resonator occupation

Here the occupation dynamics for the resonator are plotted.